Journal of Materials Processing Technology 221 (2015) 112–120

Contents lists available at ScienceDirect

Journal of Materials Processing Technology

journal homepage: www.elsevier.com/locate/jmatprotec

Formation and reduction of hydrogen porosity during selective laser melting of AlSi10Mg

Christian Weingarten[a,*], Damien Buchbinder[a], Norbert Pirch[a], Wilhelm Meiners[a], Konrad Wissenbach[a], Reinhart Poprawe[b]

[a] Fraunhofer Institute for Laser Technology (ILT), Steinbachstr. 15, D-52074 Aachen, Germany
[b] Laser Technology (LLT), RWTH Aachen University, Steinbachstr. 15, D-52074 Aachen, Germany

ARTICLE INFO

Article history:
Received 20 November 2014
Received in revised form 2 February 2015
Accepted 7 February 2015
Available online 17 February 2015

Keywords:
Selective laser melting
Aluminum
Hydrogen
Porosity
Rapid solidification

ABSTRACT

This study shows that the hydrogen porosity in AlSi10Mg parts built up with selective laser melting (SLM) can be lowered by efficient drying of the powder as well as by the modification of the process parameters. Complex structural and functional parts can be made of AlSi10Mg by SLM. Many previous investigations show that SLM with AlSi10Mg leads to high build-up rates and even better mechanical properties than casting does. But, besides all the advantages of manufacturing aluminum parts with SLM, hydrogen porosity as known from other aluminum processing methods leads to a density loss. To investigate the hydrogen porosity in SLM, cube-shaped samples were manufactured using different drying methods of the powder and varying process parameters. Regarding the density measurements, the SLM samples were evaluated to study the influence of the drying methods and process parameters on the porosity. Furthermore, the results were discussed with respect to the physical phenomena of the SLM process. In this context the physical mechanism of the hydrogen pores was investigated.

1. Introduction

Selective laser melting (SLM) is one of the additive manufacturing (AM) technologies with a powder-bed-based technique. In order to manufacture a component with SLM, the CAD model is sliced into layers typically below 150 μm thickness. Layer-by-layer the component is built up by melting the thin powder layer locally with a laser beam. Components manufactured with SLM offer a high geometrical flexibility and accuracy without almost any loss of material. This leads to resource savings and eco-design optimization. With regard to the state-of-the-art, the suitability of SLM for small series production has already been established. Over (2003) described for example the suitability of SLM for small series production of tool steel. Currently, SLM is not yet able to build up components out of cast aluminum alloys for series production cost effectively. In order to improve this efficiency, investigations were made by Buchbinder et al. (2011) to increase the build-up rate. An increase of the layer thickness or laser beam diameter is mentioned to increase the build-up rate.

A widely studied material in SLM is cast-alloy AlSi10Mg. Buchbinder (2013) showed that components of nearly 100% density can be produced of AlSi10Mg with SLM. Furthermore, Buchbinder (2013) showed that AlSi10Mg components have a wide range of mechanical properties. Thijs et al. (2013) determined that AlSi10Mg components manufactured by SLM have an extremely fine microstructure and hence a high hardness. Kempen et al. (2012) even observed higher mechanical properties of AlSi10Mg components or at least nearly the same to the cast AlSi10Mg material.

In addition to the advantageous results made on researches of SLM of AlSi10Mg, a few papers mention that spherical pores reduce the density of the components. Kempen et al. (2011) showed that this porosity is generally a consequence of entrapped gases. Our own investigations to increase the build-up rate by increasing the laser beam diameter up to $d_s = 1$ mm as well as the layer thickness up to 200 μm (laser power $P_L = 1000$ W, scan speed $v_s = 300$ mm/s) showed a density loss of greater than 10% caused by gas porosity.

Many research reports have been published on gas porosity occurring in the processing of aluminum alloys. Especially in aluminum casting or in laser welding of aluminum alloys, many methods were found to reduce the gas porosity. Kaufmann and Rooy (2004) showed this with an adjustment of the cooling rate (aluminum casting), Haboudou et al. (2003) reduced

* Corresponding author. Tel.: +49 0241 8906 282; fax: +49 0241 8906 121.
E-mail address: christian.weingarten@ilt.fraunhofer.de (C. Weingarten).

http://dx.doi.org/10.1016/j.jmatprotec.2015.02.013
0924-0136/

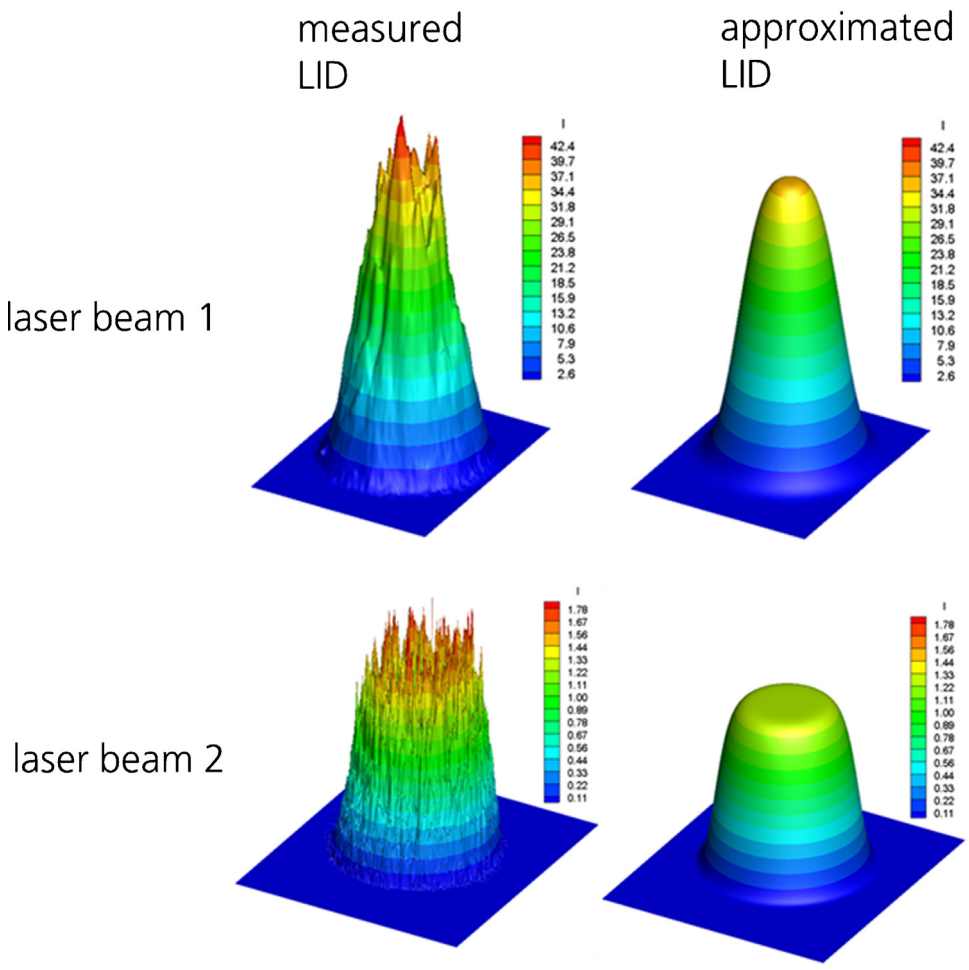

Fig. 1. Intensity distribution of the laser beam 1 and laser beam 2. Left: measured intensity distribution, right: approximation of the intensity distribution at 910 W with $n_{beam1} = 3.375$ and $n_{beam2} = 7.95$.

the gas porosity by a surface cleaning (welding). However, the results can only be transferred to the SLM process with difficulty on account of different process characteristics. For example Buchbinder et al. (2011) showed that a higher cooling rate appears in SLM (approx. 10^6 K/s) compared to conventional processes like die casting. Furthermore, typical melt pools depths d_M are smaller in SLM (approx. $d_M \approx 0.2$ mm [Buchbinder, 2013]) compared to laser welding (approx. $d_M \approx 3$ mm [Winkler (2004)]). These and other differences in the process require further investigations on the gas porosity in aluminum-alloy components manufactured by SLM.

2. Experimental details

2.1. Manufacture of samples by selective laser melting (SLM)

For the investigations all cubical samples were produced on the same SLM machine, a former Trumpf Trumaform LF250 machine. Thus, it was ensured that the individual system-related conditions such as the protective gas atmosphere or the layer preparation are identical. The machine is equipped with a diode-pumped Nd:YAG laser with maximum beam power of 1000 W. The optical system has been redesigned by ILT, both in terms of hardware and software. The machine has a circular building platform with diameter of 250 mm. The maximum measured laser power of the beam behind the optical system (scanner, collimation lens, f-θ-lens) in the working point is 910 W. The laser radiation is provided by two different optical fibers. Hence, two different laser beam diameters ($d_{s,1} = 0.3$ mm, $d_{s,2} = 1$ mm) can be used. The laser intensity distributions (LID) of the laser beams were determined by a measurement with a Spiricon® measurement system.

The results (Fig. 1, left) of the LID measurements show that the data are impaired with data noise. In order to eliminate the data noise and to characterize the LID in sufficiently high level with only a few operating figures I_0, r_0, n, the data points of the LID were approximated with this analytical function:

$$I(x,y) = I_o \times \left\{ \exp\left(-f(n) \times \left(r/r_o\right)^n\right) - C \right\}, \quad r = \sqrt{x^2 + y^2}$$
$$\text{with} \quad C = \exp\left(-f(n) \times (2)^n\right) \tag{1}$$

whereby the intensity I_0, the laser beam radius r_0 and the steepness of the slope n are derived by an approximation in the so-called quadratic medium:

$$\underbrace{\min}_{I_o, r_o, n} \sum_{j=1}^{M} \sum_{i=1}^{N} \left(I_{i,j} - I\left(x_i, y_j\right)\right) \tag{2}$$

The analytical approximation (Eq. (1)) is used for the FEM simulation of the temperature distribution in the SLM process. State of the art is to use a Gaussian distribution ($n = 2$) or a top-hat distribution ($n \approx 10$) for FEM simulations. With this approximation the LID can be characterized in detail with the steepness of the slope n.

To manufacture all of the samples, the same scan strategy was used. The scan strategy is depicted in Fig. 2. An overview of the

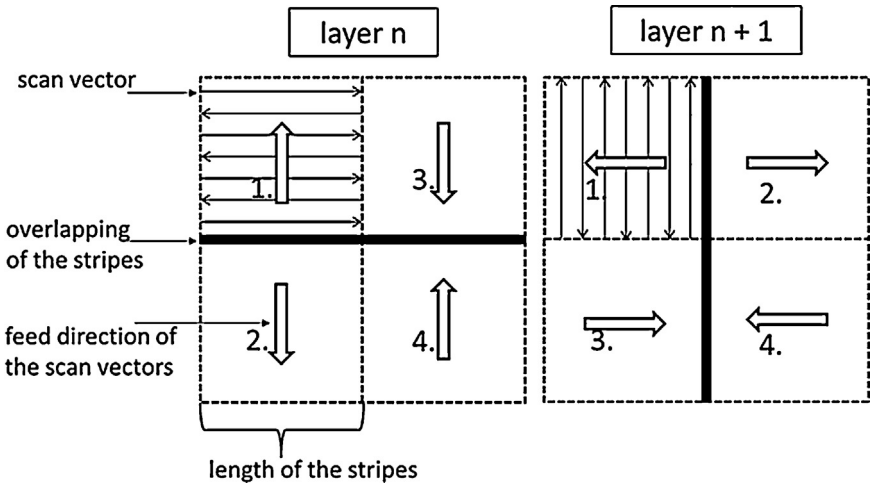

Fig. 2. Overview of the scan strategy. The numbers describe the sequence of the scanning.

Table 1
Overview of the process parameters of the manufactured samples.

Laser beam diameter (mm)	Measured laser power P_L in the working point (W)	Layer thickness d_s (μm)	Scan speed v_s (mm/s)	Hatch distance Δy_s (μm)	Edge length of the samples (mm)
$d_{s,1} = 0.3$	910	50	1000–4000	200	10
$d_{s,2} = 1$	910	50	150–350	700	20

process parameters used for manufacturing the samples is shown in Table 1.

During the process the chamber was flooded with Argon gas (DIN EN ISO 14175:I1), thereby ensuring an atmosphere with oxygen content less than 100 ppm. No platform heating was used for any of the batches.

For all investigations the same powder batch manufactured by ECKA Granules Germany GmbH was used as well. The powder has a spherical shape and size distribution of d_{10}, d_{50}, d_{90} = 20.0, 39.2, 63.6 μm. The chemical composition is shown in Table 2. The drying of the powder was performed in an industrial furnace with air atmosphere.

2.2. Methods to determine the gas content of the voids and the amount of hydrogen in the AlSi10Mg powder

To analyze the gas content of the voids in the SLM samples, three samples in a rectangular shape ($11 \times 1 \times 15\ mm^3$) were built. Subsequently, the samples were broken by a fracturing mandrel in an evacuated chamber. The released gas content was detected by a mass spectrometer. In order to measure the hydrogen content in the powder system, two different methods were applied. First, the amount of moisture on the surface of the powder particles was measured by the Karl–Fischer titration (KFT). Schöffski (2000) observed that KFT is the most widely used method for the determination of moisture content in analytical chemistry. In this process, the reaction of two reactants, running only in the presence of water, is used.

Table 2
Chemical composition of the used AlSi10Mg powder.

Alloying element	Si	Cu	Fe	Zn	Ni	Mn	Mg	Ti	Cr
wt%	9.81	0.003	0.12	0.025	0.003	0.004	0.34	0.006	0.006

The H_2O content can be determined from the spent acid solution in the range of ppb.

Second, the hot-extraction analysis (HEA) detects the total amount of hydrogen in the powder system. When the powder is heated up to solidus temperature in a vacuum atmosphere, the moisture can evaporate and the dissolved hydrogen in the aluminum can outgas. The hydrogen amount is measured with a mass spectrometer.

2.3. Material characterization methods

In this paper voids in the molten material are differentiated between gas pores and imperfections. Imperfections are caused, for example, by not completely melted powder and have a statistically geometric shape. Gas pores can be distinguished by their spherical shape (Fig. 3).

In order to determine the gas pores, cross sections parallel to the building direction z have been investigated. By means of a light

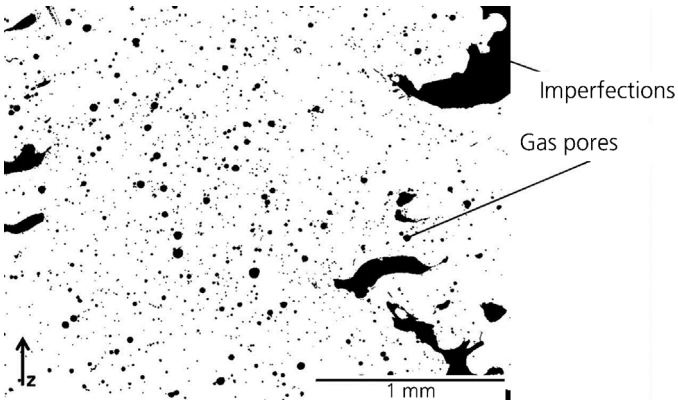

Fig. 3. Cross section of an AlSi10Mg SLM sample. The different geometric shape of imperfections and gas pores can be seen in the cross section.

Table 3
Result of the gas content analysis in voids of SLM samples by means of mass spectrometers. The resulting value based on the average value of the measurements of three samples. The values in brackets are below the detection limit.

Element	Ar	CO	CO_2	H_2	H_2O	N_2
Content in vol%	**0.27 ± 0.03**	(0.2)	(0.66)	**96 ± 2.16**	(1.2)	**1.83 ± 1.56**

microscope using a Zeiss AXIO Imager.A2m, five images distributed across the polished cross section were made. The resulting images (Fig. 4) are segmented by an image-processing program into molten material (white) and voids (black). By means of a form-factor for the roundness, the area of the pore cross-section can be determined. The gas pore density ρ_P is the quotient of the area of the gas pores and the total area. The average value of five measurements is shown in the diagrams. The standard deviation is included in the graphical representation as error bar. Due to the limited resolution of the images, only gas pores with a diameter larger 4 μm can be detected. The total density of the sample is determined by the quotient of the area of the molten material (white) and the total area.

2.4. FEM simulation

The temperature distribution in the bulk material during the SLM process will be calculated in this study by a heat conduction model. To determine the melt pool geometry, the quasi-stationary temperature field for single tracks in the solid material (AlSi10Mg) is calculated. Thereby the laser radiation is absorbed in the bulk material (absorptivity $A = 30\%$). The model is described in detail by Buchbinder (2013).

3. Results

3.1. Influence of the moisture on the gas pore density

In a first step of the examination, the gas content of the voids was studied. The results of the examination, as shown in Table 3, indicate that approx. 96% of the gas content in the voids is hydrogen. Therefore, the spherical gas pores will be identified as hydrogen pores in the further course of these investigations.

In order to determine the hydrogen sources in the SLM process, two measurements were performed. The hydrogen content of the moisture on the surface of the powder particles was measured by Karl–Fischer-Titration (KFT), which shows that a virgin powder batch contains 0.015 mass-% H_2O on the surface of the powder grains. By means of the molar mass ratio and a conversion factor, this value constitutes a hydrogen content of 18.8 ml/100 g. The total amount of hydrogen in the powder material was determined by means of the hot extraction analysis (HEA). Both the hydrogen trapped in the powder material and the hydrogen bound in the moisture are detected by the HEA. Hence, the amount of the trapped hydrogen is the difference between the result from the KFT (18.8 ml/100 g) and the HEA (33.6 ml/100 g). The resulting hydrogen amount trapped in the powder material is, thus, 14.8 ml/100 g.

This measurement shows that the maximum amount of hydrogen in the melt (33.6 ml/100 g) is approx. 50 times the amount of the solubility of hydrogen in liquid pure aluminum at melting temperature (0.7 ml/100 g [Schöffski (2000)]). Accordingly, the moisture on the surface of the powder particles is the dominating hydrogen source and has to be reduced by a drying process. The amount of trapped hydrogen in the powder material depends on the powder atomization process. This, however, will not be addressed in this paper.

Two methods are shown in this paper to reduce the moisture on the powder surface. The first method is an external drying of the powder in a furnace at a constant temperature. The influence of two different external drying temperatures ($T_{heat,1} = 90\,^{\circ}C$, $T_{heat,2} = 200\,^{\circ}C$) was studied by manufacturing SLM samples with each powder and measuring the pore density of each sample. As a reference value, SLM samples were manufactured with untreated powder as well. In Fig. 5 the pore density of the samples manufactured with SLM ($d_{s,1} = 0.3$ mm) is given in dependence of the scan speed for two drying temperatures. It is shown that the drying of the powder may reduce the porosity by up to 35% at a drying temperature of $T_{heat,1} = 90\,^{\circ}C$ and at $T_{heat,2} = 200\,^{\circ}C$ by more than 50%.

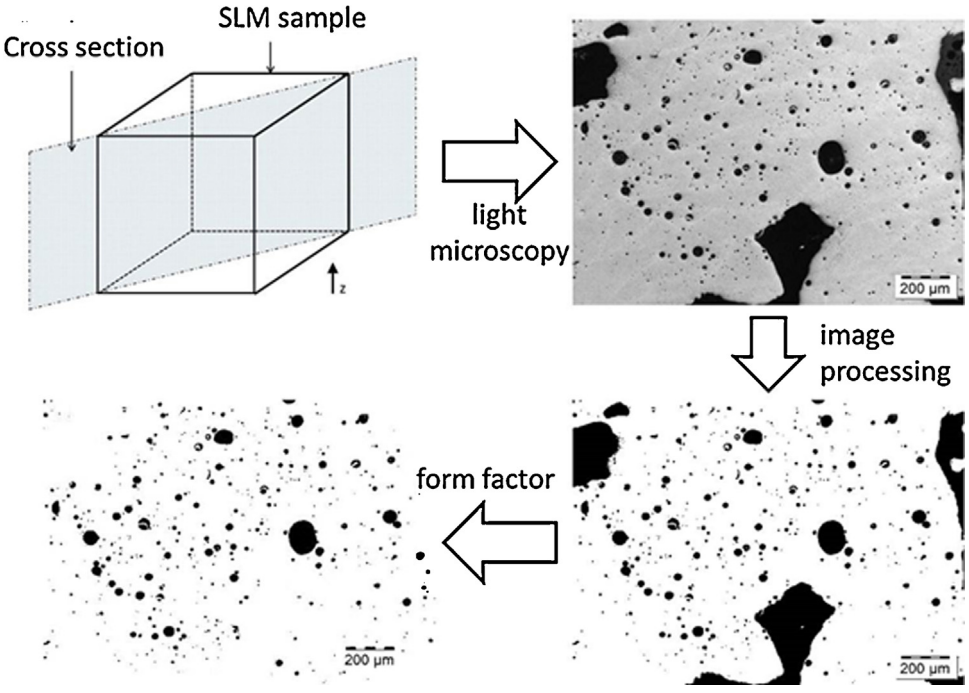

Fig. 4. Preparation of cross sections for an evaluation of gas pore density.

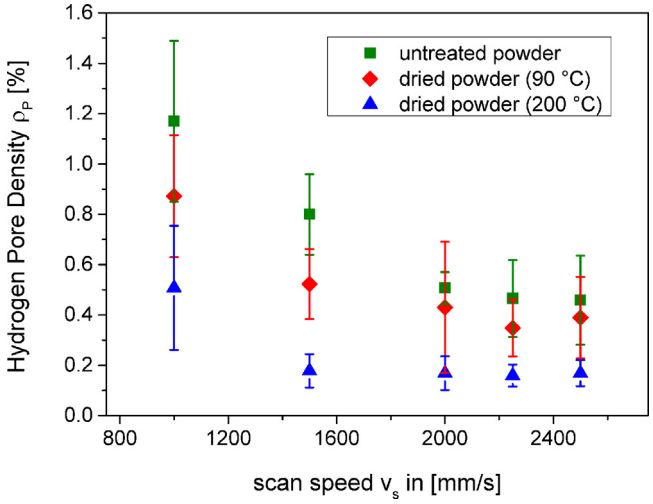

Fig. 5. Hydrogen pore density of SLM samples built up with untreated powder and dried powder depending on the scan speed for $d_{s,1}$ = 0.3 mm, P_L = 910 W.

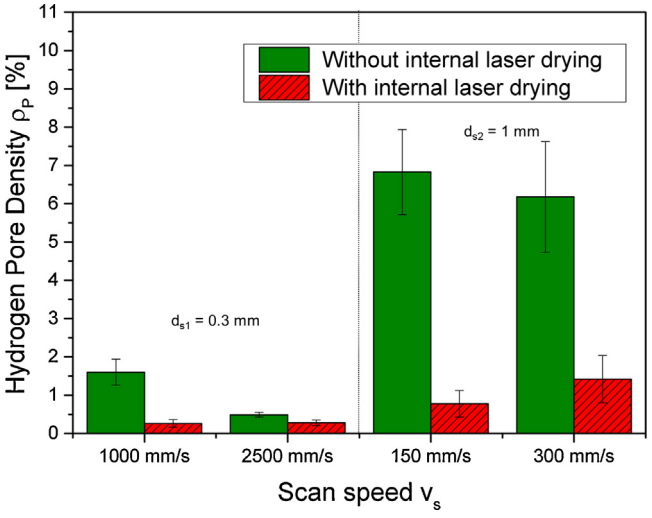

Fig. 7. Hydrogen pore density of SLM samples in dependence on the scan speed, laser beam diameter and the internal laser drying.

The second method to reduce the moisture at the powder surface is an internal laser drying. For this purpose the powder is dried during the process right after the layer deposition (Fig. 6). The heat source for the drying is laser radiation with low power. Hence, each scan vector in the layer will be scanned twice. The first scanning of the whole surface is to reduce the moisture without melting the powder. The second scanning of each scan vector is the melting process. Visual inspections show that the first scanning with a laser power of P_L = 50 W leads to a soft sintering of the powder.

In Fig. 7 the pore density of the SLM samples manufactured with an internal laser drying are compared to those SLM samples manufactured without any drying ($d_{s,1}$ = 0.3 mm, $P_{L,1}$ = 50 W, $P_{L,2}$ = 910 W). The results show that this drying method reduces the pore density from ρ_P = 1.6% to ρ_P = 0.3% when a laser beam diameter of 0.3 mm and scan speed of 1000 mm/s are used. The density of the SLM sample is raised up to over 99.5%. For a laser beam diameter of 1 mm, a density of at least 99% is achieved. Here (v_s = 150 mm/s) the pore density could be reduced up to 90% from ρ_P = 6.8% down to ρ_P = 0.8%.

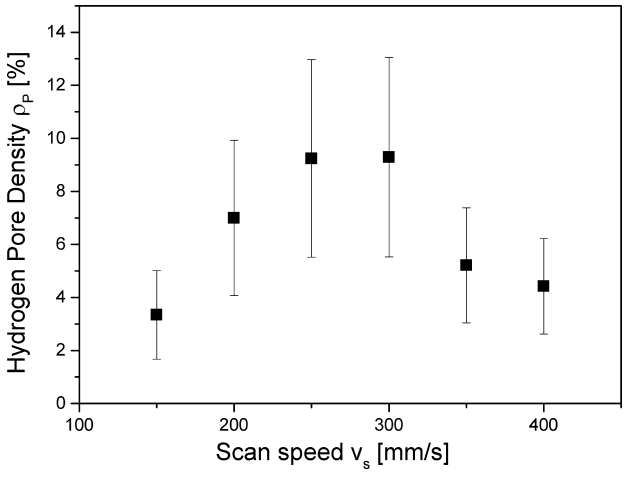

Fig. 8. Hydrogen pore density of SLM samples depending on the scan speed; $d_{s,2}$ = 1 mm, P_L = 910 W.

3.2. Influence of the scan speed on the hydrogen pore density

The influence of the scan speed while using a laser beam diameter $d_{s,1}$ = 0.3 mm is already shown in Fig. 5. An increase of the scan speed results in a decrease of the pore density. From 1000 to 2500 mm/s (without powder drying) a decrease from ρ_P = 1.2% to ρ_P = 0.5% can be achieved (Fig. 5). This is a reduction of approx. 60%.

Because the intensity decreases from approx. 12.9 to 1.2 kW/mm^2 while the laser beam diameter increases from 0.3 to 1 mm, a lower scan speed (150–350 mm/s) has to be used to manufacture SLM samples without imperfections. The scan speed used is limited by the process window to obtain sound parts without, for example, appearance of spattering or agglomeration.

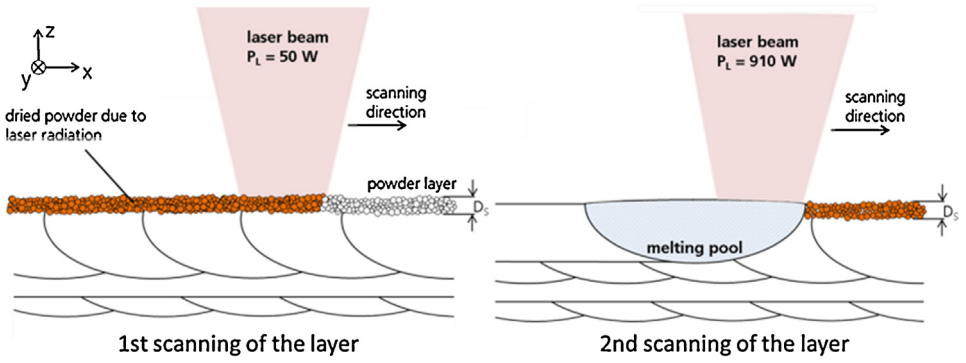

Fig. 6. Schematic illustration of the internal laser drying process.

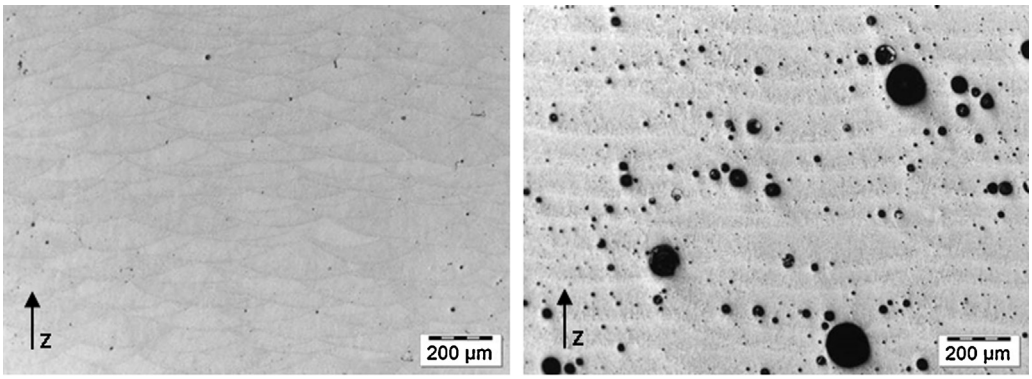

Fig. 9. Hydrogen pores in AlSi10Mg SLM samples built up with dried powder (T_{heat} = 90 °C) and a laser beam diameter of $d_{s,1}$ = 0.3 mm (v_s = 2250 mm/s, ρ_P = 0.4%) (left) and $d_{s,2}$ = 1 mm (v_s = 250 mm/s, ρ_P = 9.2%) (right).

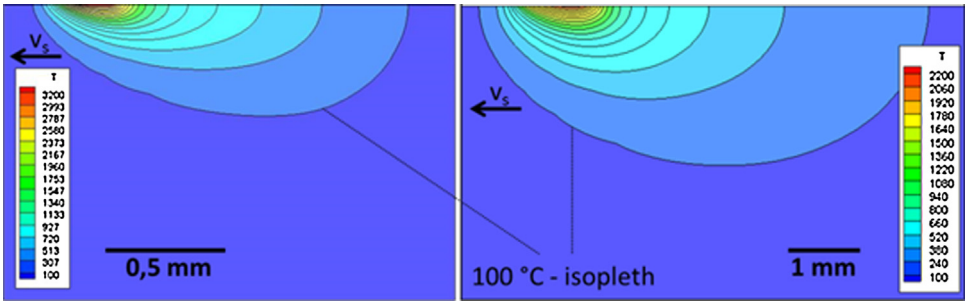

Fig. 10. Isopleth diagram of the temperature distribution in the quasi steady-state condition. Left: $d_{s,1}$ (v_s = 2000 mm/s, P_L = 910 W, A_{bulk} = 30%); right: $d_{s,2}$ (v_s = 200 mm/s, P_L = 910 W, A_{bulk} = 30%).

As seen in Fig. 8 the plot of the scan speed differs at lower values from Fig. 5. In contrast to the pore density of the samples built up with $d_{s,1}$ = 0.3 mm the pore density of the samples built up with $d_{s,2}$ = 1 mm increases from 3.3% to 9.3% for scan speed below 300 mm/s. When the span speed is raised to above 350 mm/s, gas porosity falls.

3.3. Influence of the laser beam diameter on the hydrogen pore density

For SLM samples built up with the two different beam diameters – $d_{s,1}$ = 0.3 mm and $d_{s,2}$ = 1 mm – the latter show an approx. 10-fold higher pore density (Fig. 9).

The temperature distribution of the melting process in SLM was calculated with an FEM simulation. The results are shown in Fig. 10. When the laser beam diameter $d_{s,1}$ is used, a higher local maximum temperature $T_{max,1} \approx 3200$ °C is reached. This is caused by the higher intensity. By contrast the local maximum temperature of $d_{s,2}$ $T_{max,1} \approx 2200$ °C does not reach the evaporation temperature of aluminum (T_V = 2470 °C). Another difference is the penetration depth of the heat. At $d_{s,2}$ (v_s = 200 mm/s), the heat extends deeper in to the solid material as seen at the 100 °C-isopleth. To a depth of 2 mm, the material is heated up to 100 °C. The 100 °C-isopleth, in the analytical results of $d_{s,1}$ (v_s = 2000 mm/s), is 0.41 mm, thus five times as small as the result of $d_{s,2}$.

The geometric dimensions of the melt pool can be seen in Fig. 11. The melt pool depth using $d_{s,1}$ in the analytical solution is approx. 0.15 mm and approx. 0.52 mm using $d_{s,2}$. The melt pool length amounts to 0.66 mm ($d_{s,1}$) and 1.7 mm ($d_{s,2}$). The results will be discussed in relation to the physical mechanism of the pores in Section 4.

3.4. Influence of the scan break on the hydrogen pore density

In addition to the influence of the scan speed and the laser beam diameter, the influence of the process parameter “scan break” was investigated. The scan break t_S describes the time between the end of the scan vector and the starting point of the following scan vector. When the scan break increases, the workpiece cools down, which, therefore, means there is a lower local preheating temperature of the following scan track. SLM samples with different scan breaks of 0, 25 and 50 ms were built up and analyzed for the hydrogen pore density. In Fig. 12 the results of the density measurements are exemplified for SLM samples manufactured with a

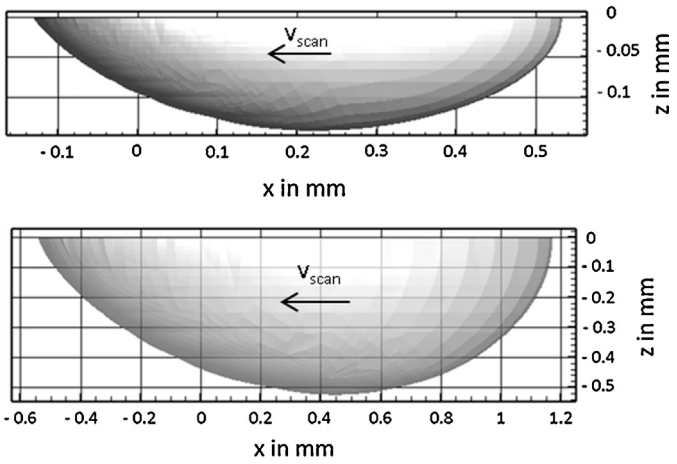

Fig. 11. Melt pool geometry in the quasi steady-state condition. Upper: $d_{s,1}$; below: $d_{s,2}$.

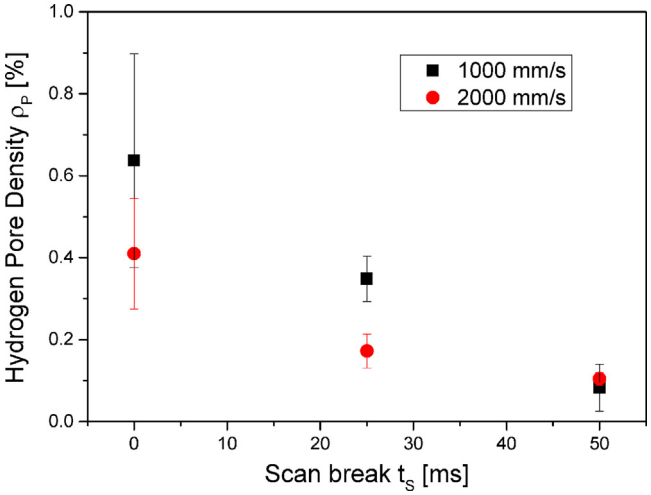

Fig. 12. Hydrogen pore density of SLM samples depending on the scan break, $d_{s,2}$ = 0.3 mm, P_L = 910 W.

laser beam diameter of 0.3 mm. This diagram shows that when the scan break is increased from 0 to 50 ms, pore density is reduced by 87% (v_s = 1000 mm/s) and 75% (v_s = 2000 mm/s).

4. Discussion

4.1. Influence of the moisture on the hydrogen porosity

The nucleation and growth of hydrogen pores occurs if the local hydrogen content is higher than the maximum solubility in liquid aluminum. The hydrogen solubility in solid pure aluminum is approx. 10-fold lower than in the liquid at the melting temperature. This means that hydrogen enriches at the solidification front if the hydrogen content in the melt is greater than the hydrogen solubility in the solid phase. As shown in the HEA of the hydrogen content in the powder, the measured value (33.6 ml/100 g) is 50-fold higher than the solubility in the melt at melting temperature (0.7 ml/100 g). Hence, if only a part of that hydrogen contamination of the powder ends up in the melt pool, the nucleation and growth of the hydrogen pores starts in the melt pool. Li and Chang (2004) described the mechanism of nucleation and growth of hydrogen porosity in solidifying aluminum alloy in with an analytical solution. In order to reduce the hydrogen porosity, the hydrogen, especially the moisture as a hydrogen source, has to be reduced.

During production, storage or handling of the powder, moisture is deposited on the powder grain surface. On the one hand, the moisture on the powder grain surface results in a poor flowability, which hinders a homogenous deposition of a thin powder layer. This is shown by Louvis et al. (2011). Fromm and Gebhard (1976) observed that on the other hand the moisture (H_2O) reacts by contact with aluminum by means of the following equation:

$$3H_2O + 2Al \rightarrow Al_2O_3 + 3H_2 \quad (3)$$

$$H_2 \rightarrow 2H_{ab} \quad (4)$$

where H_{ab} is the absorbed hydrogen in the melt.

In this work, two methods of drying the powder were shown to reduce the moisture in the process. Drying the powder in a furnace results in reduction of the porosity up to 50% (T_{heat} = 200 °C, d_s = 300 mm/s). But, the external drying temperature is limited by the sintering temperature of the AlSi10Mg powder, because agglomeration of the powder particles results in a poor flowability of the powder.

Prior to the internal laser drying process the layer preparation was carried out. Therefore, higher local drying temperatures can be achieved in the internal laser drying because agglomeration cannot affect the layer preparation. For the first time, this resulted in a density of a SLM sample up to 99% when a laser power higher than 900 W and a laser beam diameter of 1 mm was used.

In a further investigation SLM samples were built up by scanning each layer twice, but with the same laser power ($P_{L1,2}$ = 910 W). Thus, the material was melted twice (Remelting). As a result, the hydrogen porosity was reduced significantly less than it was by means of internal laser drying, which was caused when aluminum and the moisture react chemically in the melting during the first scan in the remelting process. Hence, when the powder is dried before the melting process begins, the reaction of H_2O with aluminum can be prevented.

4.2. Physical mechanism of pore growth in SLM

In addition hydrogen porosity as shown in the experiments can be reduced by changing the process parameters as well. In order to explain the results of the experiments, a closer look at a physical view of the process during melting and solidification has to be made.

In Fig. 13 the melting process is schematically shown in more detail. The laser beam moves in scanning direction and its energy absorbed by the powder. A melt pool is created, which is deeper than the layer thickness, resulting in metallurgical bonding between the layers. The solid–liquid interface consists of the melting front and the solidification front. Buchbinder (2013) showed that the local solidification speed starts with zero at the bottom of the melt pool and ends in the range of the scan speed at the melt pool surface.

The melt can be enriched with hydrogen by the interaction of the melt front and the powder particles. If the local solubility limit of the melt is reached, pore nucleation is initiated. Atwood et al. (2000) described in that the growth of the pores is diffusion controlled such that the further hydrogen supply takes place over the gaseous liquid interface of the pore. The supply rate of hydrogen is limited by the diffusion process of hydrogen within the boundary layer of the pore and the local solidification rate. That means that the growth is stopped if the pore is captured by the solidification front.

With regard to the solubility gap, it has to be considered that SLM is a rapid solidification process, which means that the partition coefficient depends on the solidification rate. So for a high solidification rate, the solubility is increased. Toda et al. (2009) described that consequently more hydrogen atoms are trapped and the solubility exceeds the equilibrium solubility of the solid phase generating a metastable state. This metastable state can relax by pore precipitation during heat treatment for precipitation hardening.

If the melt pool surface is free from oxides or other contamination, the so-called Marangoni convection is involved. If the surface tension coefficient is negative, the flow direction on the melt pool surface is directed radially outwards from the center to the melt pool boundary. This is shown by Pirch (1995) in detail. Also, Pirch (1995) showed that, the flow is able to influence the local hydrogen content along the solidification front significantly. For example, for the case above an enrichment of hydrogen in approx. two-thirds of the melting depth would be created and would thereby increase the probability for pore nucleation. For the case of high scan speeds, partial evaporation of alloying elements is, in general, involved, speeds that generate chemical gradients onto the melt pool surface and may change the sign of the surface tension coefficient. On account of this, the flow direction is reverted and the flow transports molten material with high hydrogen content from the melt pool bottom to the surface where the hydrogen can escape.

In summary, the pore formation can be reduced when the powder particle contamination with hydrogen is lowered or an adequate process management is used. When the scan speed

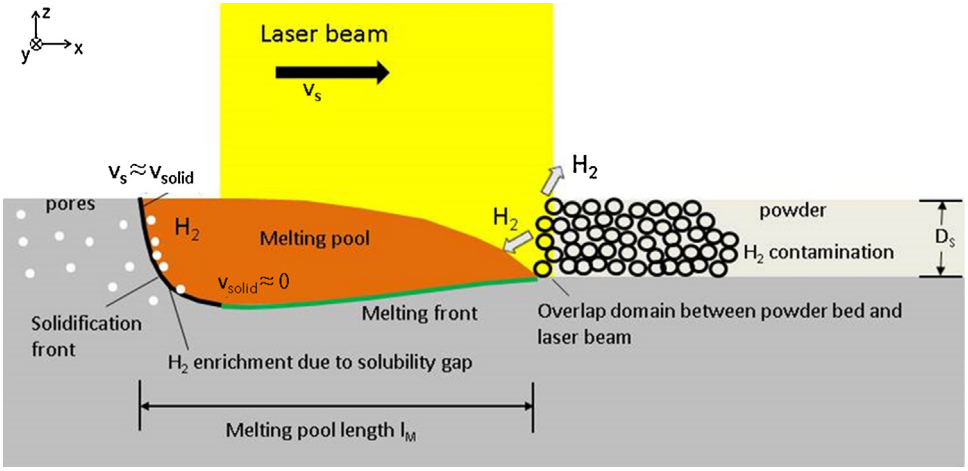

Fig. 13. Schematical overview of the interaction zone between laser radiation and powder.

is increased, the solidification increases and, thereby, the partition coefficient will be postponed to higher values generating a metastable phase. The influence of the processing strategy onto the Marangoni convection is difficult to predict because the surface tension coefficient is sensitive to the temperature and chemical composition.

The time t_M between melting and solidification is calculated by means of the following equation:

$$t_M = l_M / v_s \tag{5}$$

where l_M is the length of the melt pool and v_s the scan speed. This time is available for the pores to move up, driven by buoyancy forces, and escape, therefore, causing a reduction of the hydrogen porosity. The time t_M calculated with the results of the FEM calculation reaches a duration of 0.3 ms using $d_{s,1}$ (v_s = 2000 mm/s) and 8.5 ms using $d_{s,2}$ (v_s = 200 mm/s). The terminal velocity for the pores can be calculated by:

$$v_T = \left(\frac{2 \times g}{9 \times \eta}\right) \times r_P^2, \quad [23].$$

r_P : pore radius

η : kinematic viscosity

g : acceleration due to gravity (6)

For aluminum with a viscosity of 1.17×10^{-6} m^2/s and a pore diameter of 0.1 mm (0.05 mm), the terminal velocity is calculated to be 4.73 (1.18) mm/s. So for 8.5 ms pores with a diameter of 0.1 mm, the diameter would move up 40 μm and with 0.05 mm diameter 10 μm. This means that pores which nucleate directly at the melting front can escape by the upward movement to the melt pool surface and thereby decrease the hydrogen content. Pores which nucleate at the solidification front due to the solubility gap cannot use this mechanism because the time between nucleation and capturing by the solidification front is too short.

The temperature calculation for a scan speed of 300 mm/s shows a maximum processing temperature of about 2360 °C. So it is likely that the melt pool surface is not completely free from oxides especially at the melt pool front. This oxide layer prevents the melt from capturing the powder particles directly at the first contact, enlarges thereby the interaction time of the particles with the laser beam and increases the laser drying effect of the powder. This could also contribute to the decrease in the number of pores at scan speeds lower than 300 mm/s.

4.3. Influence of the process parameters on the hydrogen pore density

The result of the investigations as a function of the scan speed can be explained by those physical effects. In general, an increase of the scan speed results in less growth-time of the pores and in an increase of the trapped hydrogen concentration ($v_s \geq 1000$ mm/s). The pore density will be decreased. At scan speed below 300 mm/s, the pore density decreases, which is caused by the outgassing of the pores.

A scan break results in a lower local preheating and, therefore, in a decrease of the melt pool length l_M as well as in a decrease

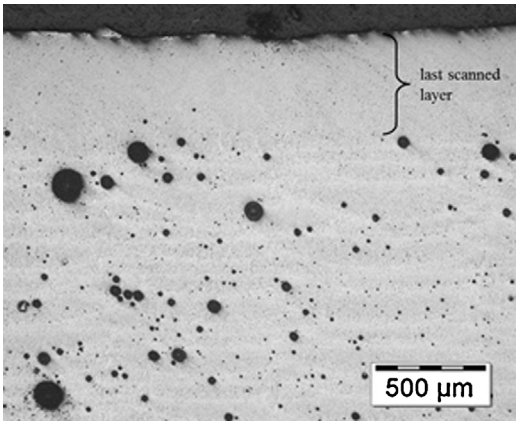

Fig. 14. Cross section of an AlSi10Mg SLM sample.

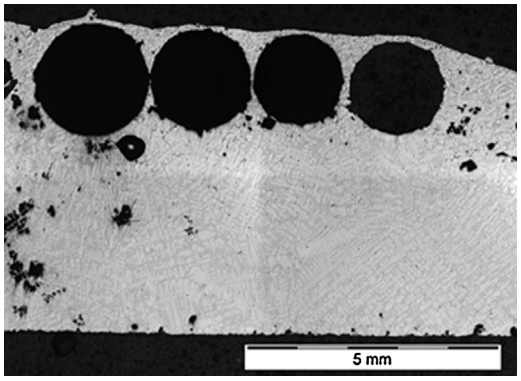

Fig. 15. Cross section of an AlSi10Mg SLM sample after a heat treatment of 1 h, 550 °C.

Table 4
Overview of the influence of the powder drying and the process parameters on the physical mechanisms and the hydrogen pore density (◯ = not specified, + = increase, – = decrease).

Process parameter/physical mechanism	Outgassing	Trapped hydrogen	Pore growth in the HAZ	Hydrogen pore density
External powder drying	◯	◯	◯	–
Internal laser drying	◯	◯	◯	–
Scan speed ($d_{s,1}$) v_{scan} > 1000 mm/s ↑	–	+	–	–
Scan speed ($d_{s,2}$) v_{scan} < 300 mm/s ↓	++	–	+	–
Scan break t_s ↑	–	+	–	–

of the time t_M. Therefore, the scan break confirms the effect which occurs at an increase of the scan speed ($v_s \geq 1000$ mm/s, see Fig. 5).

As seen in Figs. 5 and 8, SLM samples built up with a laser beam diameter of 1 mm have a significantly higher pore density than those built up with a laser beam diameter of 0.3 mm. The cause for this difference is the depth of the heat-affected zone (HAZ). With the HAZ the zone of the temperature interval below melting temperature is described, which affects the solid material in terms of recrystallization, pore growth, etc.

The HAZ is not mainly caused by the difference of the beam cross section in the focus position but by the different scan speed. In case of constant laser power, the scan speed has to be reduced by increasing the laser beam diameter to build up dense components. High scan speeds ($v_s > 1000$ mm/s) lead to a short interaction time between laser radiation and material as well as a rapid cooling. Buchbinder (2013) investigated the HAZ of SLM of AlSi10Mg using a laser beam diameter of 200 μm and scan speed of 300–2000 mm/s. No grain growth was observed and, therefore, Buchbinder (2013) excluded a HAZ by using high scan speed.

Investigation in this study suggests that the use of the laser beam diameter $d_{s,2}$ and lower scan speed in the range of 150–350 mm/s lead to the formation of a HAZ. Fig. 14 shows a cross-section of a SLM sample built up with $d_{s,2} = 1$ mm, $v_s = 200$ mm/s. It is seen that the last melted layer has a lower pore density than the rest of the cross section. This leads to the assumption that each time the following layer is scanned, the consolidated material is heat-treated. This way, the trapped hydrogen can diffuse in the already existing pore nuclei, lattice faults and grain boundaries and relax the metastable state of the lattice. Hence, the pore density increases. The FEM simulations in this study confirm this assumption due to the high temperature penetration depth beneath the melt depth. As seen in Fig. 10, the penetration depth at a lower scan speed ($v_s = 200$ mm/s) and $d_{s,2}$ is five times deeper than in the results of $d_{s,1}$ ($v_s = 2000$ mm/s). This leads to a larger HAZ and, hence, to an increase in the pore density.

For further investigation of the effect of a HAZ, a heat treatment of SLM samples in oxygen atmosphere were performed. Heat treatments of 1 h at temperatures below 525 °C do not show growth of hydrogen pores. A heat treatment at 550 °C results in growth and an ascent of the hydrogen pores to the surface as seen in Fig. 15. This result confirms the assumption that pores grow in AlSi10Mg below melting temperature in a temperature range where the yield point of the material is significantly reduced.

5. Conclusion

The moisture in the powder particle surface as well as the dissolved hydrogen in the powder material leads to a supersaturated melt. This results in nucleation and growth of hydrogen pores in the melt pool. To reduce the hydrogen porosity, the powder has to be dried. The external powder drying, limited by the agglomeration temperature of the powder particle, results in a reduction of the hydrogen porosity in SLM samples of approx. 50% ($T_{heat} = 200$ °C). When less laser power is used, an internal laser drying process enables a higher drying temperature and, therefore, a higher reduction of moisture and pore density up to 90%.

During the process the hydrogen pores can be affected by different parameters. The time between the melting and the solidification (t_M), which can be influenced e.g. by the scan speed, is a significant parameter. Because the growth of hydrogen pores is a diffusion controlled process and the diffusion rate in the melt is significant higher than in the solid material, the time t_M determines the pore size ($v_s \geq 1000$ mm/s). Since the material solidifies rapidly, the supersaturated hydrogen is trapped in the lattice. Therefore, a shorter time period, t_M, leads to a lower pore density.

Low scan speeds ($v_s \leq 300$ mm/s) can lead to an outgassing of the pores from the melt pool and in a heat affected zone as well. The heat affected zone results in a pore growth in the consolidated AlSi10Mg.

An overview of the influence of the powder drying and the process parameter on the physical mechanisms and the hydrogen pore density is shown in Table 4.

References

Atwood, R.C., Sridhar, S., Zhang, W., Lee, P.D., 2000. Diffusion-controlled growth of hydrogen pores in aluminium-silicon castings: on situ observation and modelling. Acta Mater. 48 (2), 405–417.

Buchbinder, D., 2013. Selective Laser Melting von Aluminiumgusslegierungen. Shaker Verlag, Aachen.

Buchbinder, D., Schleifenbaum, H., Heidrich, S., Meiners, W., Büttmann, J., 2011. High power selective laser melting (HP SLM) of aluminium parts. Physics Procedia 12, 271–278.

Fromm, E., Gebhard, E., 1976. Gase und Kohlenstoffe in Metallen. Springer, Berlin.

Haboudou, A., Peyre, P., Vannes, A.B., Peix, G., 2003. Reduction of porosity content generated during Nd:YAG laser welding of A356 and AA5083 aluminium alloys. Mater. Sci. Eng. 363, 40–52.

Kaufmann, J.G., Rooy, E.L., 2004. Aluminum Alloy Castings: Properties, Processes, and Applications. ASM International, Ohio, USA.

Kempen, K., Thijs, L., Van Humbeeck, J., Kruth, J.-P., 2012. Mechanical properties of AlSi10Mg produced by selective laser melting. Physics Procedia 39, 439–446.

Kempen, K., Thijs, L., Yasa, E., Badrossamay, M., Verheecke, W., Kruth, J.P., 2011. Microstructural analysis and process optimization for selective laser melting of AlSi10Mg. In: Proceedings Solid Freeform Fabrication Symposium, Texas, USA.

Li, K.-D., Chang, E., 2004. Mechanism of nucleation and growth of hydrogen porosity in solidifying A356 aluminum alloy: an analytical solution. Acta Mater. 52, 219–231.

Louvis, E., Fox, P., Sutcliffe, C.J., 2011. Selective laser melting of aluminium components. J. Mater. Process. Technol. 211, 275–284.

Over, C., 2003. Generative Fertigung von Bauteilen aus Werkzeugstahl X38CrMoV5-1 und Titan TiAl6V4 mit "Selective Laser Melting". Shaker Verlag, Aachen.

Pirch, N., 1995. Randschichtlegieren von Aluminiumwerkstoffen mit Laserstrahlung: physikalische Prozesse, Modelle und Integrationsverfahren. RWTH, Aachen (RWTH Aachen Thesis).

Schöffski, K., 2000. Die Wasserbestimmung mit Karl–Fischer Titration. Chemie in unserer Zeit. 34 (3), 170–175.

Thijs, L., Kempen, K., Kruth, J.-P., Van Humbeeck, J., 2013. Fine-structured aluminium products with controllable texture by selective laser melting of pre-alloyed AlSi10Mg powder. Acta Mater. 61, 1809–1819.

Toda, H., Hidaka, T., Kobayashi, M., Uesugi, K., Takeuchi, A., Horikawa, K., 2009. Growth behavior of hydrogen micropores in aluminum alloys during high-temperature exposure. Acta Mater. 57, 2277–2290.

Winkler, R., 2004. Porenbildung beim Laserstrahlschweissen von Aluminium-Druckguss. UTZ, Munich.